Electronic Supplementary Information

Transparent nature-based luminescent solar concentrator with NIR emission and integrated thermal sensing

Sandra F.H. Correia,*[a] Bruno Falcão, [b] Gonçalo Figueiredo, [b, c] Bárbara M. C. Vaz, [d] Letícia S. Contieri, [d, e] Leonardo M. de Souza Mesquita, [d, e] Juliana Almeida, [f, g] Joana C. Fradinho, [f, g] Diana C. G. A. Pinto, [h] Lianshe Fu, [b] Paulo S. André, [c] Sónia P. M. Ventura, [d] Vitor Sencadas *[i] and Rute A. S. Ferreira [b]

*sandracorreia@av.it.pt; vsencadas@ua.pt

[a.] Instituto de Telecomunicações and University of Aveiro, Campus Universitário de Santiago, 3810-193 Aveiro, Portugal.

[b.] Department of Physics and CICECO - Aveiro Institute of Materials, University of Aveiro, 3810-193 Aveiro, Portugal.

[c.] Department of Electrical and Computer Engineering and Instituto de Telecomunicações, Instituto Superior Técnico, University of Lisbon, 1049-001 Lisbon, Portugal.

[d.] Department of Chemistry and CICECO - Aveiro Institute of Materials, University of Aveiro, 3810-193 Aveiro, Portugal.

[e.] Multidisciplinary Laboratory of Food and Health (LabMAS), School of Applied Sciences (FCA), University of Campinas, Rua Pedro Zaccaria 1300, 13484-350, Limeira, Sao Paulo, Brazil

[f.] Associate Laboratory i4HB - Institute for Health and Bioeconomy, NOVA School of Science and Technology, NOVA University of Lisbon, 2829-516 Caparica, Portugal

[g.] UCIBIO - Applied Molecular Biosciences Unit, Department of Chemistry, NOVA School of Science and Technology, NOVA University Lisbon, 2829-516 Caparica, Portugal

[h.] LAQV – REQUIMTE, Department of Chemistry, University of Aveiro, 3810-193 Aveiro, Portugal

[i.] Department of Materials and Ceramic Engineering and CICECO - Aveiro Institute of Materials, University of Aveiro, 3810-193 Aveiro, Portugal.

Experimental details

Chemical compounds. Ethanol (HPLC grade, CAS 64-17-5), and acetone (HPLC grade, CAS 67-64-1) used in the extraction of BChl were acquired from Fisher Scientific. Dimethyl ether (99 wt% of purity, CAS 115-10-6) was supplied by Sigma-Aldrich. The surfactants, sodium dodecylsulfate, SDS (pharma grade, CAS 151-21-3), and polyethylene glycol sorbitan monolaurate, Tween 20 (CAS 9005-64-5), were purchased by Panreac, and Sigma-Aldrich, respectively. Dodecyltrimethylammonium bromide, $[N_{1,1,1,12}]Br$ (99 wt% of purity, CAS 1119-94-4) and tetradecyltrimethylammonium bromide, $[N_{1,1,1,14}]Br$ (98 wt% of purity, CAS 1119-97-7), were acquired from Alfa Aesar while decyltrimethylammonium bromide, $[N_{1,1,1,10}]Br$ (99 wt% of purity, CAS 2082-84-0), were purchased from Tokyo Chemical Industry. The tributyltetradecylphosphonium chloride, $[P_{4,4,4,14}]Cl$ (95 wt% of purity), and 1-dodecyl-3-methylimidazolium chloride, $[C_{12}C_1im]Cl$ (98 wt% of purity, CAS 114569-84-5) were supplied by IoLiTec. Chloroform (Puriss ph. Eur. 99.0 – 99.4% GC) was purchased at Honeywell and SEBS (Calprene H6180X, with 85/15 ethylene butylene/styrene ratio) at Dynasol Group.

Phototrophic mixed cultures operation. Activated sludge from Beirolas wastewater treatment plant (Lisbon, Portugal), was enriched in phototrophic purple bacteria under photoheterotrophic conditions and used as the inoculum for the cultivation of the phototrophic mixed culture (PMC) used in this study. The PMC was selected under 24 h cycles and the permanent presence of an organic and an inorganic carbon source (butyric acid and carbonate, respectively), in a 4.2 L sequencing batch reactor (SBR) at a temperature of 30 °C. The reactor was continuously illuminated through external illumination provided by four halogen lamps (2 lamps of 100W; 2 lamps of 53W), at a light intensity of 90.9 $W.m^{-2}$, corresponding to a volumetric intensity of 2.34 $W.L^{-1}$. A UV-Visible absorbing filter (Lee Colour Filter 299 1.2 N.D.) was covering the reactor walls, limiting the light input to NIR wavelengths. The SBR was fed at the beginning of the cycle with a synthetic solution of butyric acid (133 mL, organic loading rate of 35 $Cmmol.L^{-1}.day^{-1}$), mineral medium (133 mL containing *per* liter: 3.12 g of $MgCl_2 \cdot 6H_2O$, 0.43 g of $MgSO_4 \cdot 7H_2O$, 8.42 g of NaCl, 9.29 g of NH_4Cl, 1.05 g of $CaCl_2 \cdot 2H_2O$, 105 mL of iron citrate solution (1.0 $g.L^{-1}$), 21 mL trace element solution) and phosphate medium (1 L containing *per* liter: 0.16 g of KH_2PO_4 and 0.20 g of K_2HPO_4). The inorganic carbon feeding was performed twice in the cycle, with the first feeding at the beginning of the cycle and the second feeding occurring after 12 h of a cycle (66 mL *per* feeding, containing *per* liter 10 g of Na_2CO_3). The reactor was operated under continuous magnetic stirring and with an HRT and a SRT of 3 days, established through mixed liquor withdrawal of 1.4 L at the end of each cycle. pH was controlled at 6.5 using HCl (1 M) and NaOH (1 M).

The biomass used for this study was freshly collected from the 1.4 L withdrawal of the reactor and centrifuged at 10 000 g, for 30 minutes at room temperature. The supernatant was discharged, and the biomass pellets were stored at -20°C until further processing. The biomass collection occurred for 2 weeks until 10 g of biomass was recovered.

BChl extraction. Several solvents were used to test the extraction of BChl, including ethanol at 50% (v/v), pure acetone, and dimethyl ether. In addition, aqueous solutions of cationic tensioative ionic liquids, anionic, and non-ionic surfactants at 250 mM with a solid-liquid ratio (SLR) of 0.05 $g_{wet\ biomass}.mL_{solvent}^{-1}$ were also investigated. The extraction was performed in a digital shaker (IKA Trayster) under a vertical rotation of 80 rpm at room temperature (20 – 25 °C) for 30 min and protected from light exposure. After that, a centrifugation step was employed in a Thermo Scientific Heraeus Megafuge 16R centrifuge at 4700 *g*, for 30 min at 4 °C. The /MSbiomass debris was discarded while the supernatant was collected. Then, for the preparation of the BChl films, the solvent was removed from the supernatant using a rotary evaporator, allowing to obtain dry BChl and ready to be used afterwards. When necessary, the dried extract was redissolved in 5 mL of dichloromethane for further analysis. The quantification of BChl was performed by recording the absorption spectra between 300 and 800 nm using a UV-Vis microplate reader (Synergy HT microplate reader – BioTek). Then, it was calculated the extraction efficiency ($\%_{Relative}$)

over the best extraction solvent (considering 100% of the extraction efficiency) at 775 nm for organic solvents, and 757 nm for aqueous solutions of tensioactive compounds.

Quality of the transmitted light

One of the main applications for LSCs is their use as building windows, and thus LSC devices should not distort the spectrum of the natural light to ensure that the transmitted light meets basic indoor activities [1]. The transmitted light is often assessed by the Average Visible Transmission (AVT) parameter, which is dependent on the photopic response of the human eye:[2]

$$AVT = \frac{\int T(\lambda)P(\lambda)AM1.5G(\lambda)d(\lambda)}{\int P(\lambda)AM1.5G(\lambda)d(\lambda)} \quad \text{(S1)}$$

where $T(\lambda)$ is the transmission spectra (Fig. S13a), P(λ) is photopic response of the human eye and AM1.5G(λ) is the solar photon flux spectrum (photons·s^{-1}·m^{-2}).

To quantify the colour appearance of the planar LSCs and their effects on colour perception, the transmitted light was analysed in terms of CIE 1931 colour space diagram coordinates and colour rendering index (CRI) which evaluated the ability to accurately render the colour of objects (Fig. 4d and Fig. S13b in Supporting Information). The CRI is evaluated on a 0 to 100 scale, with a CRI above 70 being considered good quality and above 95 of excellent quality.[2, 3]

LSCs performance evaluation parameters

Due to size constraints that prevent the performance evaluation of the LSC using an integrating sphere, the external photon efficiency (η_{ext}) (also commonly known as optical conversion efficiency, η_{opt}) was estimated through electrical parameters obtained from the edge-coupled PV devices applied to Equation S2:[4]

$$\eta_{ext} = \frac{P_{out}}{P_{in}} = \frac{I_{SC}^{L} V_{oc}^{L} A_e \eta_{solar}}{I_{SC} V_{oc} A_s \, \eta_{PV}} \quad \text{(S2)}$$

where P_{out} and P_{in} are the output and incident optical power, respectively, I_{SC}^{L} and V_{oc}^{L} represent the short-circuit current and the open-circuit voltage when the PV device is coupled to the LSC, I_{sc} and V_{oc} are the corresponding values of the PV device exposed directly to solar radiation and A_s and A_e are the exposed and total edge areas respectively. We should note that following the guidelines recently presented as standard protocols,[5, 6] the spectral mismatch between the response of edge-mounted PV cells and the LSC emission was corrected through inclusion of the η_{solar} and η_{PV} parameters which correspond to the efficiency of the PV device relative to the total solar spectrum and is the efficiency of the PV device at the LSC emission wavelengths, respectively. Three measurements were performed for each case, with a relative error ($\eta_{opt}/\Delta\eta_{opt}$) found to be below 10 %.

The experimental η_{ext} values were determined by illuminating the top surface of the LSCs with AM1.5G illumination from a solar simulator. The optical power at the LSC output was estimated using an array of commercial c-Si PV cells (KXOB22-01X8F, IXYS) coupled to three edges of the LSC. The I_{sc} and V_{oc} values were measured using a current source meter device (2400 SourceMeter SMU Instruments, Keithley). All measurements were performed under AM1.5G illumination (1000 W·m^{-2}) using a 150 W xenon arc lamp, class A, solar simulator (Model 10500, Abet Technologies). The device efficiency (η_{dev}), which is often known as power conversion efficiency (PCE), was calculated through Equation S3:

$$\eta_{dev} = \frac{P_{out}^{el}}{P_{in}} = \frac{I_{SC}^{L} V_{oc}^{L} FF}{A_S \int_{\lambda_1}^{\lambda_2} I_{AM1.5G}(\lambda) d\lambda} \quad \text{(S3)}$$

where P_{out}^{el} and FF = 0.75 are the PV device output electrical power and fill factor of the PV cell, respectively.

Optical and structural properties

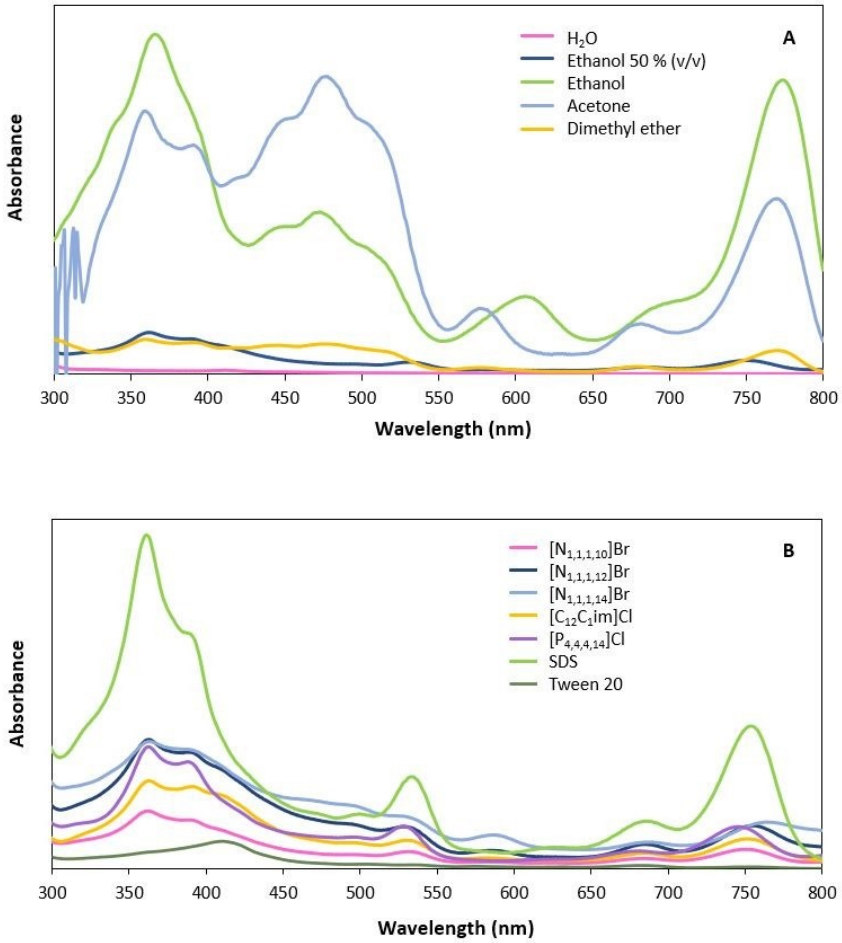

Fig. S1. UV-Vis spectroscopy of the extracts obtained after the extraction of BChl with different solvents at 250 mM and SLR of 0.05 $g_{wet\ biomass}.mL_{solvent}^{-1}$.

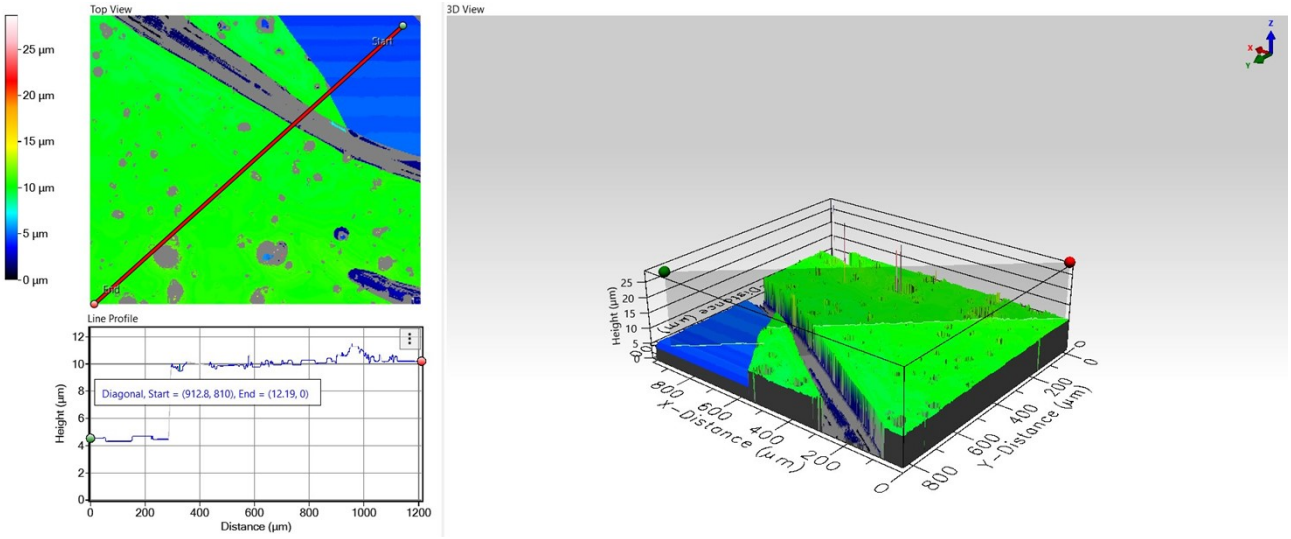

Fig. S2. Profilometry thickness measurement results of the BChl/SEBS LSC.

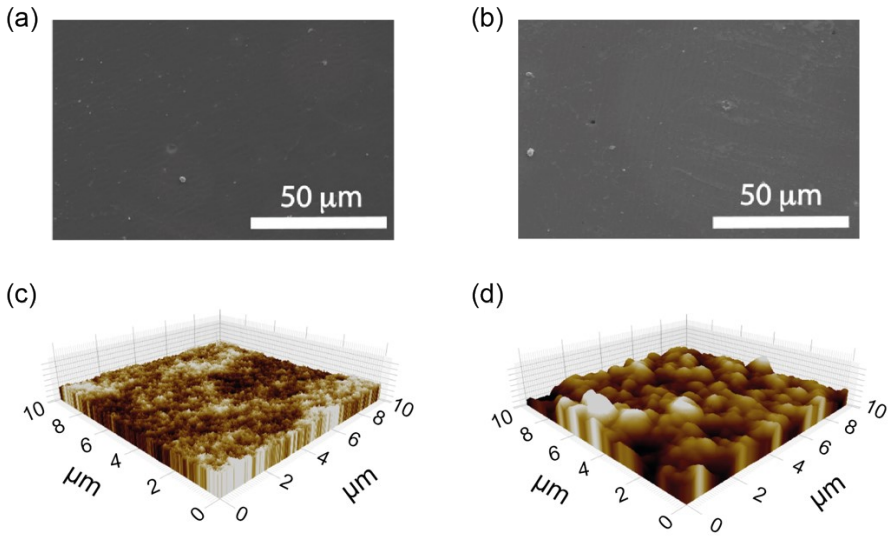

Fig. S3. Scanning electron microscopy images of (a) BChl/SEBS-1 and (b) BChl/SEBS-4. Atomic force microscopy images of (c) SEBS and (d) BChl/SEBS-2.

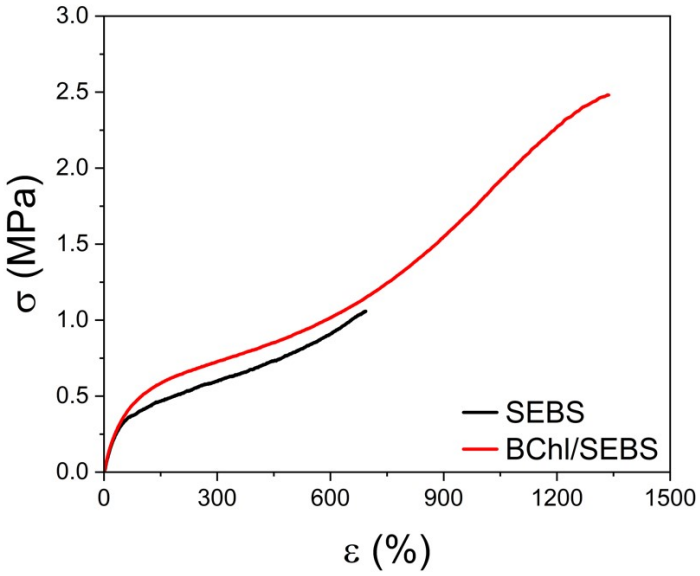

Fig. S4. Stress-strain behavior of the SEBS and BChl/SEBS samples.

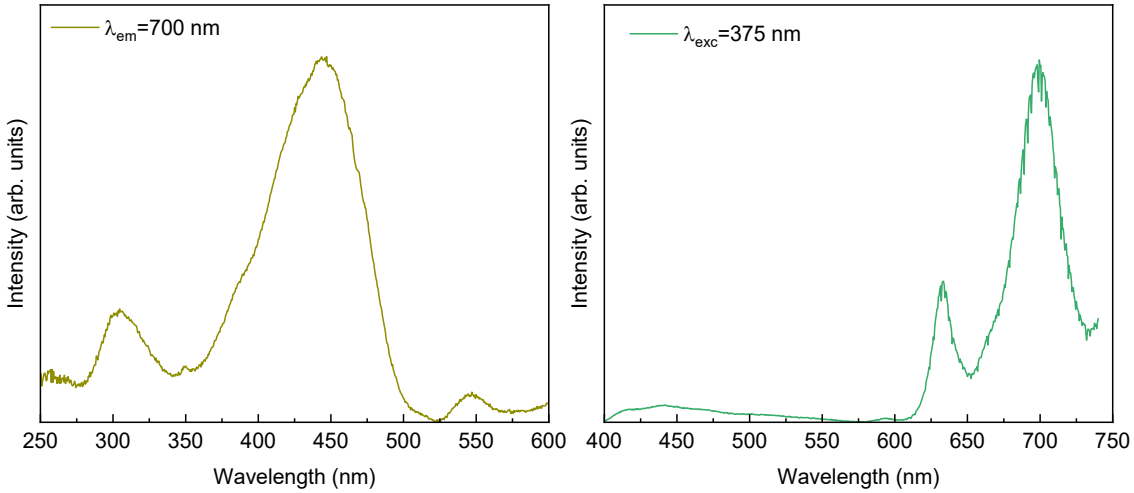

Fig. S5. Room-temperature excitation (left) and emission (right) spectra of BChl in ethanolic solution.

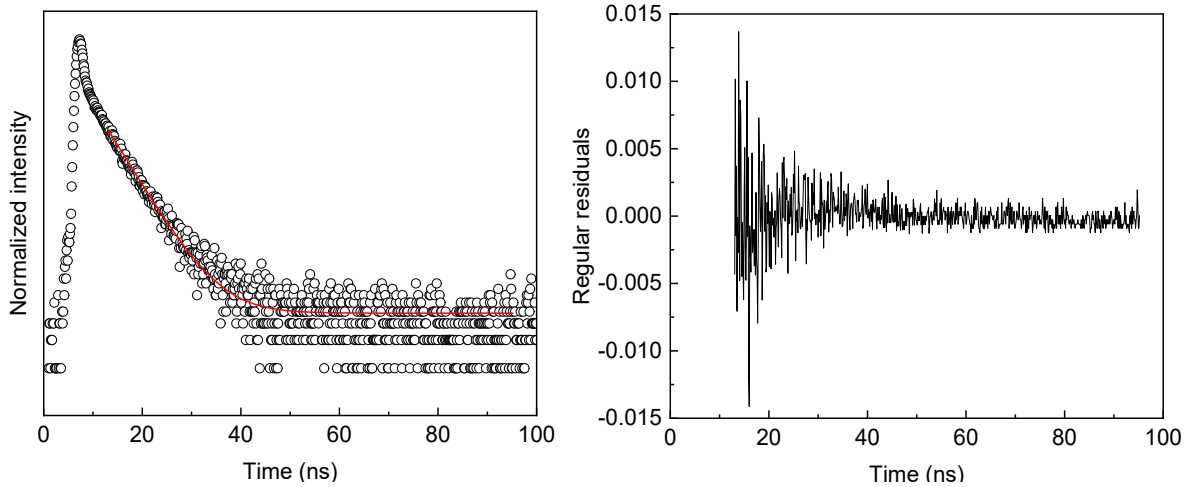

Fig. S6 Room-temperature emission decay curve of BChl/SEBS-1 excited at 390 nm and monitored at 700 nm. The solid line represents the data best fit ($R^2 > 0.99$), using a single-exponential function $I(t) = I_1 e^{-(t-t_0)/\tau_1}$. The emission lifetime τ_1 was estimated to be 5.06 ± 0.04 ns. The respective residual plot is shown on the right-hand side.

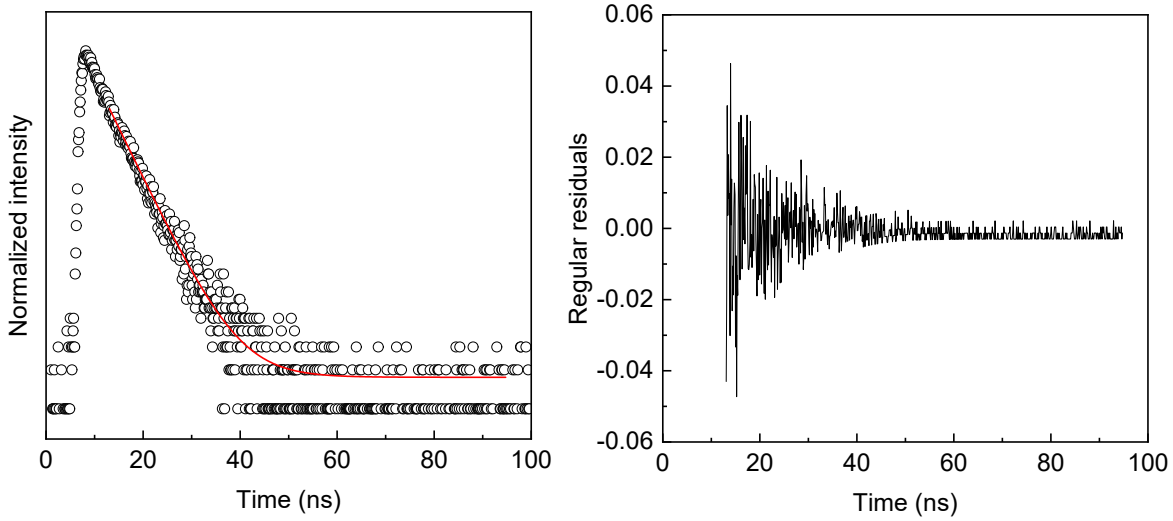

Fig. S7. Room-temperature emission decay curve of BChl/SEBS-2 excited at 390 nm and monitored at 700 nm. The solid line represents the data best fit ($R^2 > 0.99$), using a single-exponential function $I(t) = I_1 e^{-(t-t_0)/\tau_1}$. The emission lifetime τ_1 was estimated to be 5.58 ± 0.04 ns. The respective residual plot is shown on the right-hand side.

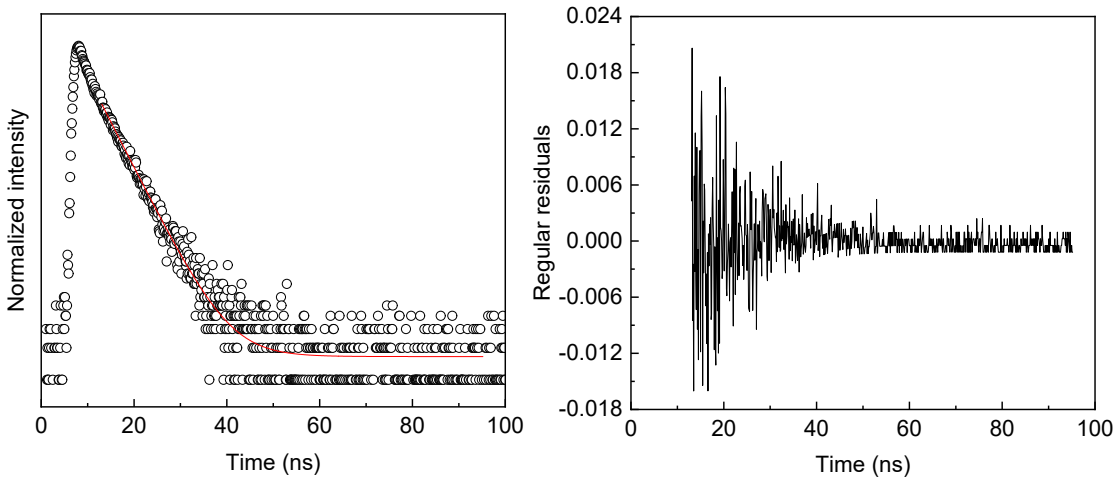

Fig. S8. Room-temperature emission decay curve of BChl/SEBS-3 excited at 390 nm and monitored at 700 nm. The solid line represents the data best fit ($R^2 > 0.99$), using a single-exponential function $I(t) = I_1 e^{-(t-t_0)/\tau_1}$. The emission lifetime τ_1 was estimated to be 5.04 ± 0.03 ns. The respective residual plot is shown on the right-hand side.

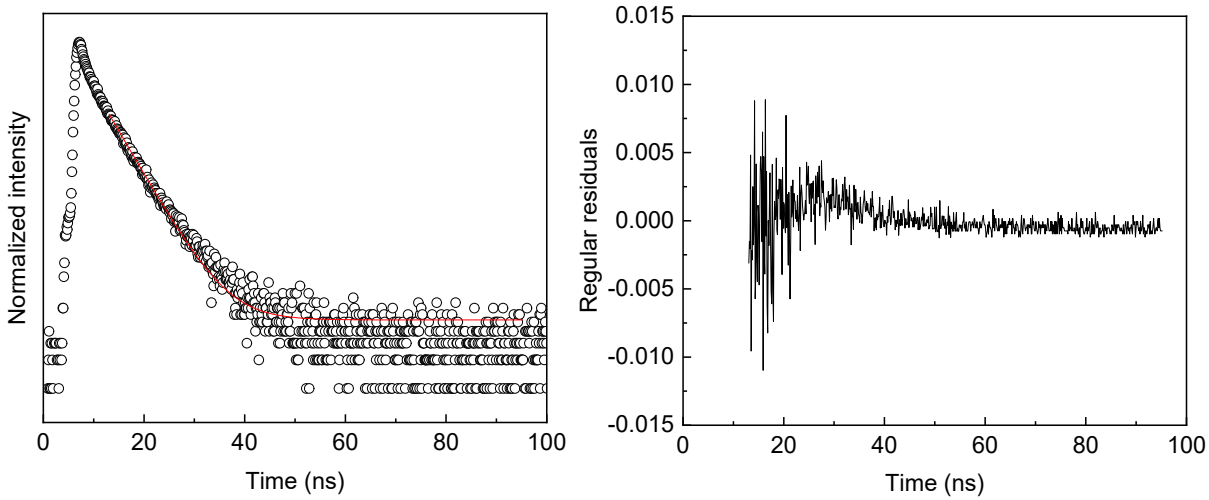

Fig. S9. Room-temperature emission decay curve of BChl/SEBS-4 excited at 390 nm and monitored at 700 nm. The solid line represents the data best fit ($R^2 > 0.99$), using a single-exponential function $I(t) = I_1 e^{-(t-t_0)/\tau_1}$. The emission lifetime τ_1 was estimated to be 4.74 ± 0.01 ns. The respective residual plot is shown on the right-hand side.

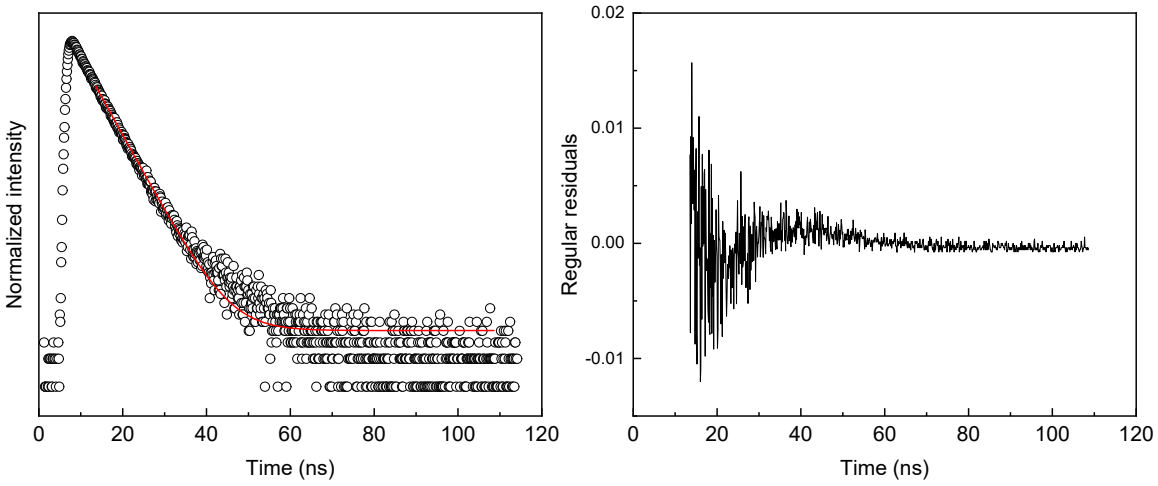

Fig. S10. Room-temperature emission decay curve of BChl ethanolic extract excited at 390 nm and monitored at 700 nm. The solid line represents the data best fit ($R^2 > 0.99$), using a single-exponential function $I(t) = I_1 e^{-(t-t_0)/\tau_1}$. The emission lifetime τ_1 was estimated to be 5.30 ± 0.01 ns. The respective residual plot is shown on the right-hand side.

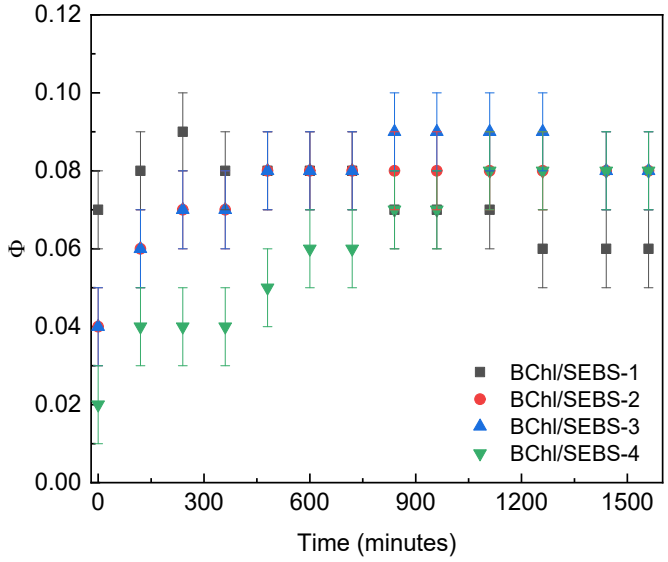

Fig. S11. Absolute emission quantum yield (Φ) values of BChl/SEBS-X (X=1,2,3,4) samples as function of exposition time to AM1.5G solar simulator (λ_{exc}= 415/420 nm).

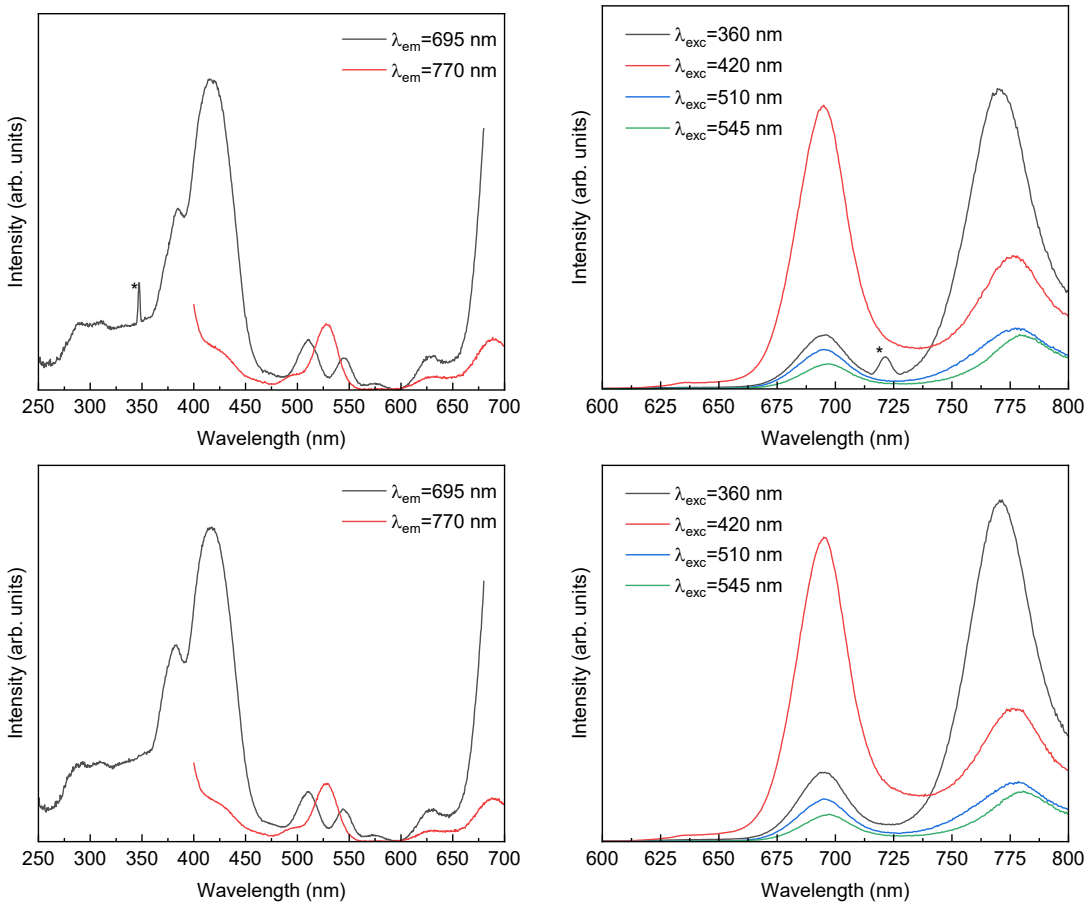

Fig. S12. Room-temperature excitation (left) and emission (right) spectra of BChl/SEBS-2 before (top) and after (bottom) exposition to T=25ºC/RH=95%.

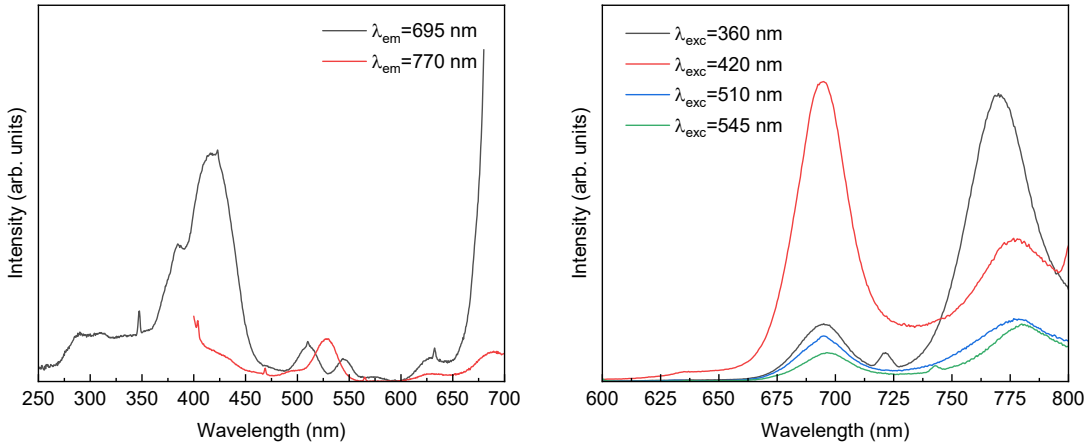

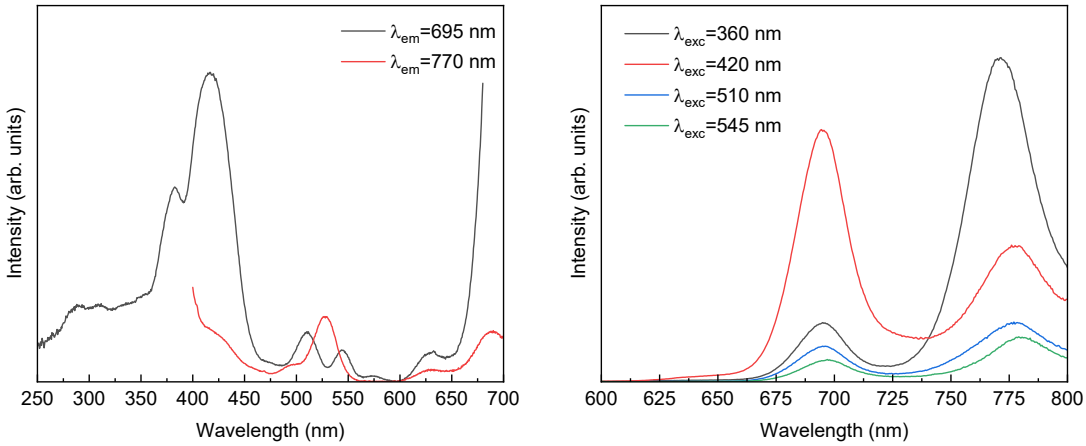

Fig. S13. Room-temperature excitation (left) and emission (right) spectra of BChl/SEBS-2 before (top) and after (bottom) exposition to T=50ºC/RH=60%.

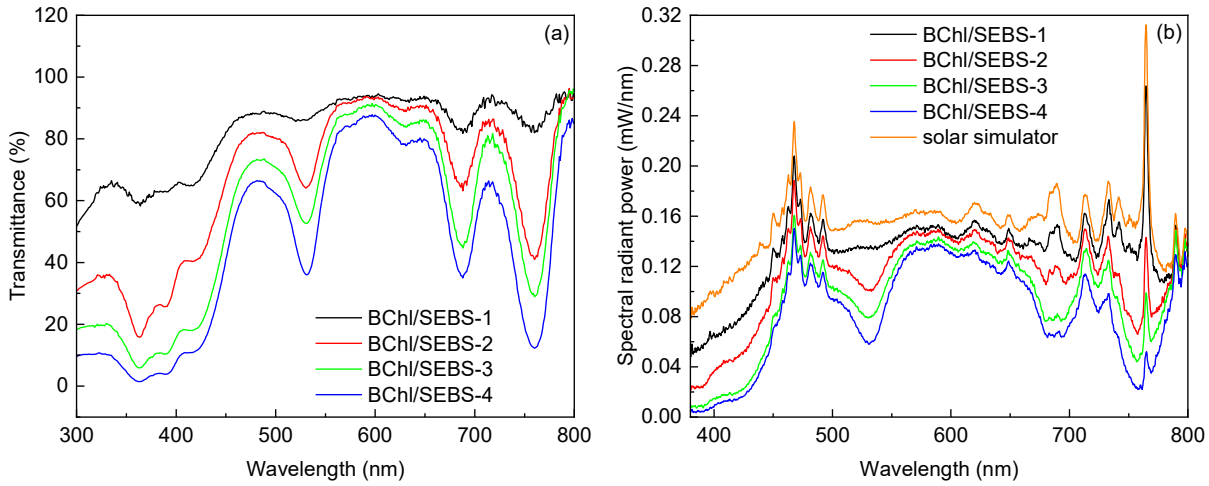

Fig. S14. (a) Transmittance spectra of BChl/SEBS samples and (b) spectra of the transmitted light of the BChl/SEBS-X (X=1,2,3,4) samples under AM1.5G solar simulator.

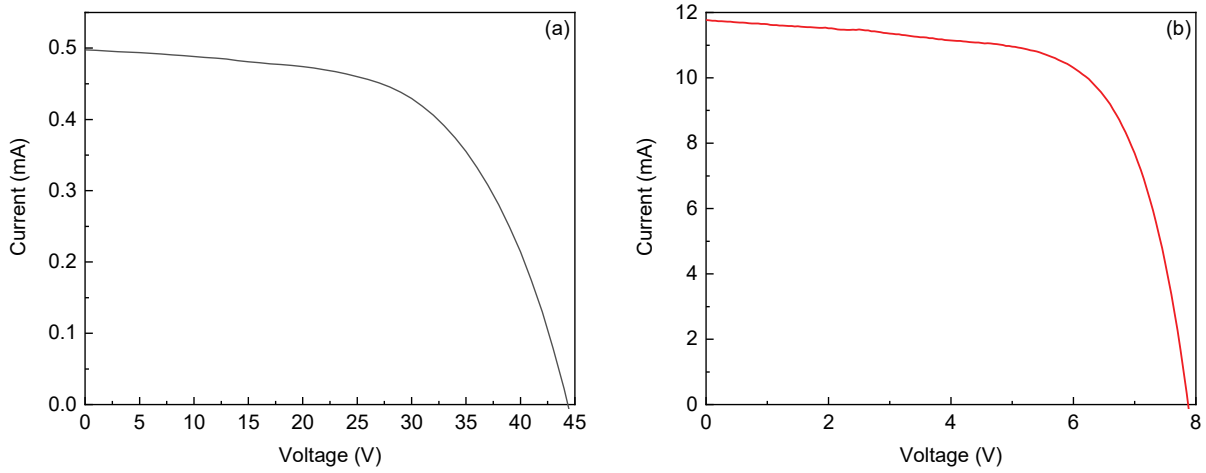

Fig. S15. I-V curves of the PV cells directly exposed to simulated AM1.5G solar radiation for the (a) 10.5×10.5×0.8 cm^3 and (b) 38×28×0.8 cm^3 BChl/SEBS LSC prototypes.

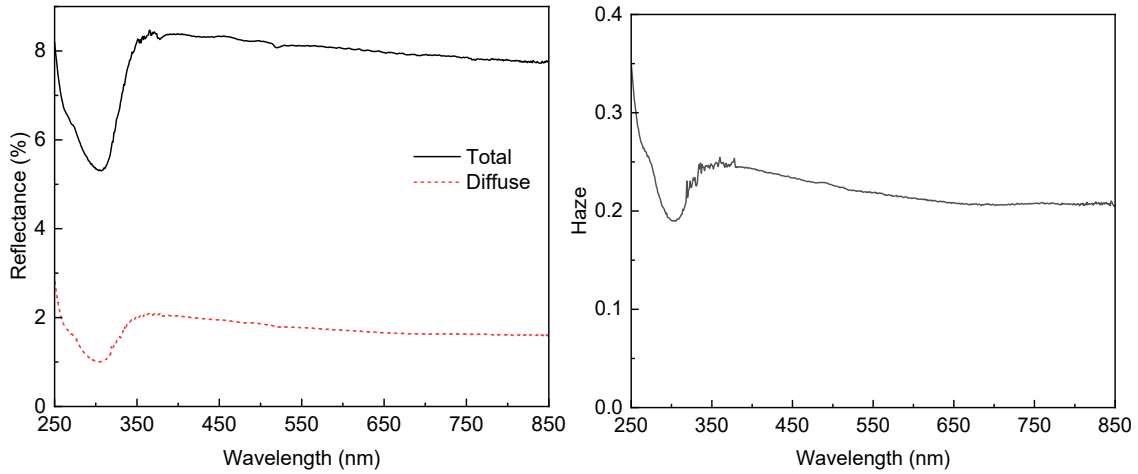

Fig. S16. (a) Total and diffuse reflectance and (b) haze factor of the BChl/SEBS LSC. The haze factor was determined as the ratio of diffuse reflectance to total reflectance.

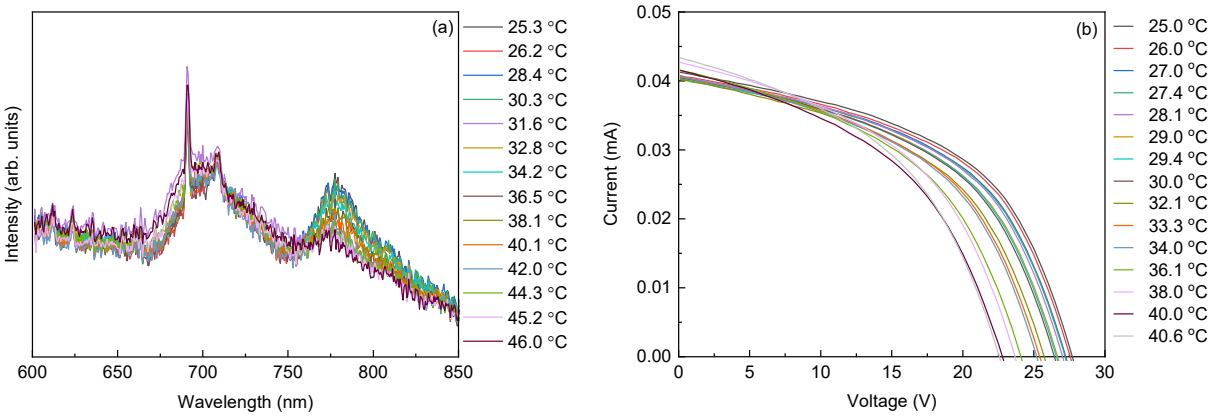

Fig. S17. (a) Emission spectra of the LSC based on BChl/SEBS under simulated AM1.5G radiation and (b) I-V curves of the PV cells coupled to the edges of the BChl/SEBS as function of the temperature.

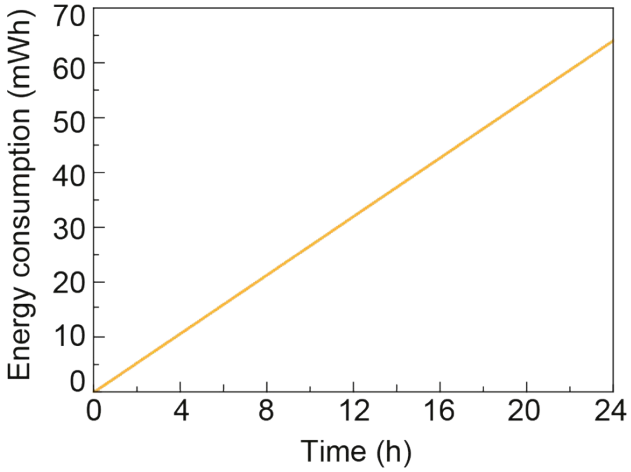

Fig. S18. Energy consumed by the components of an IoT system able to measure and transmit the data from the LSC prototypes.[7]

Tables

Table S1. Composition of the BChl ethanolic extract at 470 nm performed by UHPLC-DAD-ESI/MS.

Compound	Retention time (min)	$[M-H]^-$ (*m/z*)	UV-Vis (nm)	Compound abundance (%)
Chl *b* derivative with Zn and two OH	12.36	983	219, 304, 453, 658	22.8
Chl *a* derivative with Zn and two OH	12.54	967	219, 310, 462, 671	15.3
Chl *a* derivative with Zn and two OH	12.93	1012	220, 310, 462, 672	11.8
Chl *b* derivative	13.10	951	221, 316, 457, 666	10.3
BChl *a* derivative of Zn	13.20	1015	261, 365, 597, 671, 771	11.8
BChl *a* derivative	15.60	903	357, 521, 748	5.1

Table S2. Composition of the ethanolic extract at 750 nm performed by UHPLC-DAD-ESI/MS.

Compound	Retention time (min)	$[M-H]^-$ (*m/z*)	UV-Vis (nm)	Compound abundance (%)
BChl *a* derivative of Zn	13.25	1015	263, 364, 596, 684, 769	22.8
BChl *a* derivative	13.65	999	267, 366, 595, 771	11.3
BChl *a* derivative of Zn	13.87	1015	260, 366, 589, 679, 778	3.8
BChl *b* derivative	14.74	795	356, 523, 742	1.8
BChl *a* derivative	15.60	903	357, 521, 748	26.6
BChl *b* derivative	15.95	596	357, 523, 748	11.2
BChl *b* derivative	17.35	885	357, 525, 744	2.0
BChl *b* derivative	17.49	930	357, 521, 746	3.7

Table S3. Composition of the SDS extract at 450 nm performed by UHPLC-DAD-ESI/MS.

Compound	Retention time (min)	$[M-H]^-$ (*m/z*)	UV-Vis (nm)	Compound abundance (%)
Chl *b* derivative	13.72	902	413, 679	2.0
Chl *b* derivative	13.88	902	414, 679	3.8
Chl *a* derivative	14.81	916	436, 672	10.6
BChl *a* derivative	15.62	903	357, 471, 515, 747	13.6
BChl *a* derivative	16.32	887	357, 526, 724	15.6

Table S4. Absolute emission quantum yield (*q)* measured at 420 nm), for the BChl/SEBS-2 sample before and after the photodegradation tests in a climatic chamber at distinct temperature (T) and relative humidity (RH) conditions.

T (°C)	RH (%)	*q*	
		before	**after**
50	60	0.02 ± 0.01	0.02 ± 0.01
25	95	0.02 ± 0.01	0.02 ± 0.01

References

1. D. M. Liu, Y. Y. Sun, R. Wilson and Y. P. Wu, *Renew. Energ.*, 2020, **145**, 1399-1411.

2. T. A. de Bruin and W. G. J. H. M. van Sark, *Front. Phys.*, 2022, **10**, 856799.

3. H. Wu, L. Ying, W. Yang and Y. Cao, in *WOLEDs and Organic Photovoltaics*, ed. V. W. W. Yam, Springer, Berlin, Heidelberg, 2010, pp. 37–78.

4. R. Reisfeld, D. Shamrakov and C. Jorgensen, *Sol. Energ. Mat. Sol. C.*, 1994, **33**, 417-427.

5. M. G. Debije, R. C. Evans and G. Griffini, *Energ. Environ. Sci.*, 2021, **14**, 293-301.

6. C. C. Yang, H. A. Atwater, M. A. Baldo, D. Baran, C. J. Barile, M. C. Barr, M. Bates, M. G. Bawendi, M. R. Bergren, B. Borhan, C. J. Brabec, S. Brovelli, V. Bulovic, P. Ceroni, M. G. Debije, J. M. Delgado-Sanchez, W. J. Dong, P. M. Duxbury, R. C. Evans, S. R. Forrest, D. R. Gamelin, N. C. Giebink, X. Gong, G. Griffini, F. Guo, C. K. Herrera, A. W. Y. Ho-Baillie, R. J. Holmes, S. K. Hong, T. Kirchartz, B. G. Levine, H. B. Li, Y. L. Li, D. Y. Liu, M. A. Loi, C. K. Luscombe, N. S. Makarov, F. Mateen, R. Mazzaro, H. McDaniel, M. D. McGehee, F. Meinardi, A. Menendez-Velazquez, J. Min, D. B. Mitzi, M. Moemeni, J. H. Moon, A. Nattestad, M. K. Nazeeruddin, A. F. Nogueira, U. W. Paetzold, D. L. Patrick, A. Pucci, B. P. Rand, E. Reichmanis, B. S. Richards, J. Roncali, F. Rosei, T. W. Schmidt, F. So, C. C. Tu, A. Vahdani, W. G. J. H. M. van Sark, R. Verduzco, A. Vomiero, W. W. H. Wong, K. F. Wu, H. L. Yip, X. W. Zhang, H. G. Zhao and R. R. Lunt, *Joule*, 2022, **6**, 8-15.

7. G. Figueiredo, S. F. H. Correia, B. P. Falcão, V. Sencadas, L. Fu, P. S. André and R. A. S. Ferreira, *Adv. Sci.*, 2024, **11**, 2400540.